LETTER

doi:10.1038/nature10203

# Deep winds beneath Saturn's upper clouds from a seasonal long-lived planetary-scale storm

A. Sánchez-Lavega[1], T. del Río-Gaztelurrutia[1], R. Hueso[1], J. M. Gómez-Forrellad[2], J. F. Sanz-Requena[3], J. Legarreta[4], E. García-Melendo[2,5], F. Colas[6], J. Lecacheux[7], L. N. Fletcher[8], D. Barrado-Navascués[9], D. Parker[10] & the International Outer Planet Watch Team*

**Convective storms occur regularly in Saturn's atmosphere[1–4]. Huge storms known as Great White Spots, which are ten times larger than the regular storms, are rarer and occur about once per Saturnian year (29.5 Earth years). Current models propose that the outbreak of a Great White Spot is due to moist convection induced by water[5,6]. However, the generation of the global disturbance and its effect on Saturn's permanent winds[1,7] have hitherto been unconstrained[8] by data, because there was insufficient spatial resolution and temporal sampling[9–11] to infer the dynamics of Saturn's weather layer (the layer in the troposphere where the cloud forms). Theoretically, it has been suggested that this phenomenon is seasonally controlled[5,9,10]. Here we report observations of a storm at northern latitudes in the peak of a weak westward jet during the beginning of northern springtime, in accord with the seasonal cycle but earlier than expected. The storm head moved faster than the jet, was active during the two-month observation period, and triggered a planetary-scale disturbance that circled Saturn but did not significantly alter the ambient zonal winds. Numerical simulations of the phenomenon show that, as on Jupiter[12], Saturn's winds extend without decay deep down into the weather layer, at least to the water-cloud base at pressures of 10–12 bar, which is much deeper than solar radiation penetrates.**

Ground-based telescopes detected the first signs of the storm on 5 December 2010 at 21:05:22 Universal Time (UT), when a barely visible bright point emerged on Saturn at planetographic latitude 37.7 ± 0.8° N (Fig. 1). This is nearly simultaneous with the detection of electrical activity linked to the storm at 19:18 UT by the Radio Plasma Wave Science (RPWS) instrument on board the Cassini spacecraft[13], when considering the travel time of light from Saturn to Earth (80 min) at this epoch. As in previous Great White Spot (GWS) outbreaks[5,9,14,15], the spot grew rapidly both in size and brightness, expanding from a length of ~3,000 km to 8,000 km in just one week. Following this expansion, the spot was centred at latitude 41.1 ± 1.1° N, and had a rotation period about Saturn of 10 h 41 min 43.6 s, implying a westward zonal wind speed of −28.7 ± 0.2 m s$^{-1}$ in the System III reference frame[16]. Two weeks after the outbreak, the GWS disturbance consisted of a bright compact spot (the 'storm head') followed to the east by a zonally expanding tail of bright clouds between latitudes 30° N and 45° N (Fig. 2). This tail formed a planetary-scale disturbance that encircled the planet in 55 days. The shape of the head of the storm and its drift rate remained unperturbed following its encounter with the disturbance, a behaviour consistent with the drag of the disturbance clouds by ambient zonal winds, in a similar way to that observed in the last GWS event on Saturn's equator in 1990[9–11,15].

Tracking individual cloud elements (sizes ~1,000–3,000 km) during the observing period (5 December 2010 to 19 February 2011) allowed us to derive their motions (Fig. 3; see also Supplementary Information). The drift rate of the head of the storm did not change in this period; it moved westwards 10 m s$^{-1}$ faster than the westward-jet peak velocity.

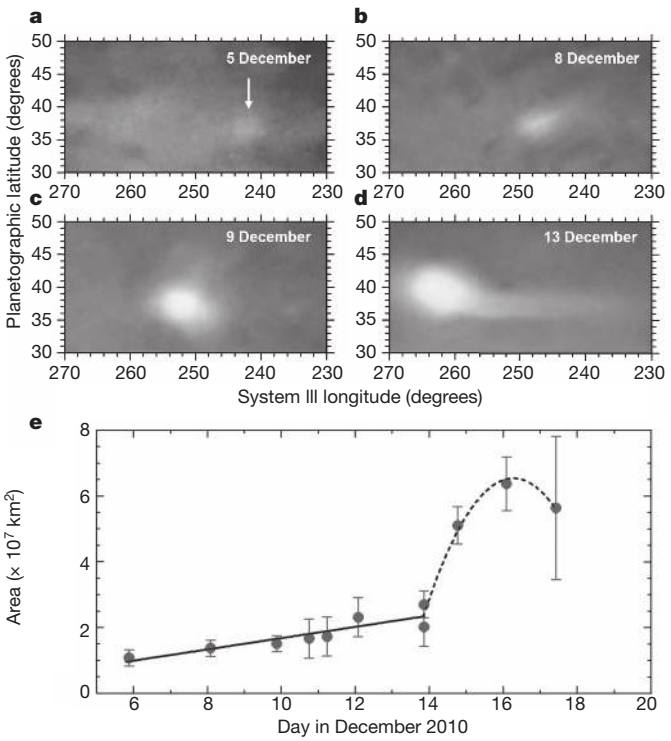


**Figure 1 | Initial growth of the Great White Spot.** **a**–**d**, Map projections of the storm clouds obtained on 5 December (**a**, by T.I.), 8 December (**b**, by S.G.), 9 December (**c**, by T.K.) and 13 December (**d**, by C.G.). Measurement of the area occupied by the bright core (without considering the southern tail in the later images) is shown in **e**. Solid and dashed lines are respectively linear and parabolic fits to the area growth rate. During the first 13 days after onset, the growth rate was d$A$/d$t$ = 20 km$^2$ s$^{-1}$; during the next two days, the growth rate was d$A$/d$t$ = 212 km$^2$ s$^{-1}$. The images used in this study were obtained in the visible range (wavelengths 350 nm–954 nm) by a large number of observers contributing to the IOPW-PVOL database[30] and the ALPO-Japan database (details are given in Supplementary Information). Multi-spectral photometric images were obtained at the 1-m telescope at Pic-du-Midi Observatory (France), the 2.2-m telescope at Calar Alto Observatory (Spain), and a 0.41-m telescope (D.P.). Error bars show the r.m.s. corresponding to several measurements of the storm area over each image.

[1]Departamento de Física Aplicada I, Escuela Técnica Superior de Ingeniería, Universidad del País Vasco, Alameda Urquijo s/n, 48013 Bilbao, Spain. [2]Esteve Duran Observatory Foundation, 08553 Seva, Spain. [3]Universidad Europea Miguel de Cervantes, C/Padre Julio Chevalier, 47012 Valladolid, Spain. [4]Departamento de Ingeniería de Sistemas y Automática, EUITI, Universidad País Vasco, Plaza de la Casilla 3, 48012 Bilbao, Spain. [5]Institut de Ciències de l'Espai (CSIC-IEEC), Campus UAB, Facultat de Ciències, Torre C5, parell, 2a pl., E-08193 Bellaterra, Spain. [6]Institut de Mécanique Céleste et de Calcul des Ephémérides, Observatoire de Paris, UMR 8028 CNRS, 77 av. Denfert-Rochereau, 75014 Paris, France. [7]Observatoire de Paris, LESIA, 5, Place Jules Janssen, 92195 Meudon Cedex, France. [8]Atmospheric, Oceanic and Planetary Physics, Department of Physics, Clarendon Laboratory, University of Oxford, Parks Road, Oxford OX1 3PU, UK. [9]Observatorio de Calar Alto, Centro Astronómico Hispano Alemán, MPIA-CSIC, 04004 Almería, Spain. [10]Association of Lunar and Planetary Observers (ALPO), 12911 Lerida Street, Coral Gables, Florida 33156, USA.
*Lists of participants and their affiliations appear at the end of the paper.

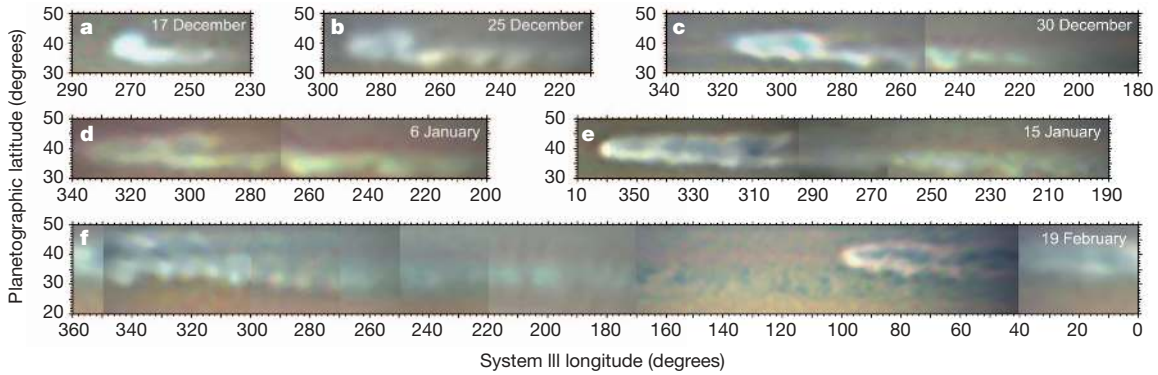


**Figure 2 | Expansion of the storm clouds and the planetary-scale disturbance.** Maps were made by assembling images from different observers (see Supplementary Information). The storm head moved westward (left in the maps), and showed a bow shape consistent with the meridional zonal wind profile. **a**–**c**, The bright clouds forming the southern branch of the disturbance (between latitudes 38° and 30° N, in a region of cyclonic vorticity) progressed eastward. Later on 22 December, a northern branch developed (latitudes 40° to 45° N, anticyclonic vorticity), which also progressed eastward (**d**, **e**). In about two months the disturbance encircled the planet, and the southern branch elements, moving in the opposite direction, encountered the head of the storm on 29 January, 4° southward in latitude (**f**). The eastward expansion in longitude of the disturbance's central branch (between latitudes 40° and 42°) formed dark spots, one of which was persistent (probably an anticyclonic vortex) at latitude 41.9° ± 1.3° (s.d.) with a size of ~4,000 km (System III longitude 308° in **e**). Small bright spots in the southern part of the disturbance at latitudes 35° to 38° N showed a periodic distribution with a dominant zonal wavelength of 15.7° ± 3° (**b**–**f**) and survived for a maximum of approximately two weeks.

On the other hand, disturbance features moved in the zonal direction with speeds very close to those of the ambient winds. Therefore winds at the upper cloud level, which have remained essentially unchanged throughout a whole Saturn year[1,7], were not altered by the disturbance at this early stage.

Observations obtained with a variety of filters—from the ultraviolet (375 nm) to the near-infrared (954 nm), including the deep methane absorption band at 883 nm—showed that the GWS was brighter than the adjacent undisturbed area at the same latitude by ~10% at 375 nm, 19% at 450 nm, 25% at 537 nm, 16% at 580 nm and 11% at 630 nm (see Supplementary Information). At 375 nm, Rayleigh scattering contributes to the brightness, but at the other wavelengths free of the gaseous methane absorption, brightness is essentially controlled by the storm particles[17], suggesting that the storm injects fresh ice particles into the tropopause, where they mix with the pre-existing haze. In order to retrieve the vertical cloud structure of the storm, we used a standard

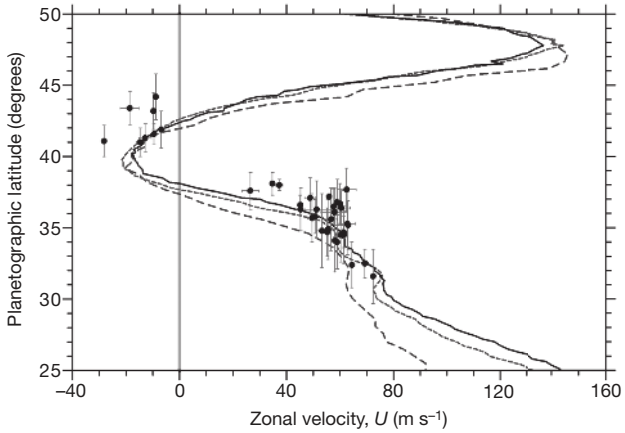


**Figure 3 | Zonal winds from motions of the disturbance clouds.** Data points correspond to wind speed measured for single tracers pertaining to the disturbance (Supplementary Information). The storm head corresponds to the point with the highest westward velocity ($-28.7\ m\ s^{-1}$). The lines represent wind profiles; long-dashed line, obtained during the encounters of the Voyager spacecraft in 1980–81 (ref. 7); and using Cassini images at two altitude levels within the tropospheric haze (solid line) and upper cloud (short dashed) in 2004–09. The latitude uncertainty for the points is ±1.3° (s.d.); the wind speed uncertainty is $\pm 0.2\ m\ s^{-1}$ (s.d.) for the storm head, and ranges from ±0.5 to $\pm 2\ m\ s^{-1}$ (s.d.) for other features.

three-layer radiative transfer model for Saturn[18–20]. The model atmosphere consisted of a stratospheric haze of thin Mie particles of size ~0.1 μm located between 2 and 60 mbar, and a dense tropospheric haze extending from 0.1 bar down to the ammonia cloud deck at 1.4 bar. We found that the GWS was embedded within the tropospheric haze, with its cloud tops located at ~150 mbar—that is, 3 km below the top of the haze, and 20 km below the tropopause, which is located near 100 mbar, according to thermal infrared measurements[21].

The rapid growth and high brightness of the GWS core, together with the abundant electric activity detected by Cassini RPWS instrument[13], are consistent with previous proposals that these events are moist convective storms driven by condensation of ammonia and water (at the 1–2 bar and 10–12 bar levels, respectively)[5,6]. Flow divergence at the top of the ascending motions can be related to the growing area $A$ of the storm (Fig. 1) through mass continuity by $\nabla\bullet\mathbf{V} = (1/A)(dA/dt) = (1\text{–}5) \times 10^{-6}\ s^{-1}$ (where $\mathbf{V}$ is the horizontal velocity). This implies a vertical velocity ($w$) at the cloud top of the storm of $w \leq h \cdot \nabla\bullet\mathbf{V} \approx 2.5\ m\ s^{-1}$, where $h = 260$ km is the vertical length of the path followed by the ascending convective parcels from altitude (pressure $P$) levels $P_{bottom} \approx 10$ bar (water clouds) to $P_{top} \approx 0.1$ bar (the tropopause). However, deep moist convection in Saturn is vigorous in the core of the ascending convective towers[5,6], and to first order the maximum vertical velocity $w_{max}$ can be related to the convective available potential energy (CAPE) by $\mathrm{CAPE} = \int_{z_1}^{z_2} g \frac{\Delta T}{T(z)} dz = \frac{w_{max}^2}{2}$, where $g$ is the acceleration due to gravity and $\Delta T$ is the temperature difference between the ascending parcel and the ambient (which has vertical temperature profile $T(z)$). Assuming a constant $\Delta T$ of just 1 K, this results in $w_{max} = \sqrt{2\mathrm{CAPE}} \approx \left(2g \frac{\Delta T}{<T>} h\right)^{1/2} \approx 150\ m\ s^{-1}$ for $g = 10\ m\ s^{-2}$ and mean temperature $<T> = 250$ K. Given the high vertical velocities, the large vertical extent of the core of the GWS, and its enormous horizontal size (of the order of the width of the mid-latitude jets), this huge disturbance serves as a tool to diagnose the dynamics of Saturn's weather layer, which ranges from the deep troposphere (10 bar) to 0.01 bar or higher in the stratosphere.

In order to explain the structure of the disturbance at cloud level, we ran nonlinear simulations of the response of Saturn's upper troposphere and stratosphere to a steady vertical heat source that tries to mimic the GWS convective storm head using the EPIC code[22]. We tested the structure of the atmosphere by varying the zonal wind

vertical profile and the thermal structure in a forward modelling of the potential vorticity (PV) field[23]. As both the PV and the cloud field are considered to act as passive tracers of the flow, we sought the PV field evolution that best reproduced the observed cloud morphology. Figure 4 shows results from a simulation of the first 12 days of the PV field that closely resembles the evolution of the cloud disturbance (compare to Fig. 2a–c in this work, and to figure 3 in ref. 13). These successful simulations require a weather layer with a very low static stability, $N^2 = 0.03 \times 10^{-4}\,s^{-2}$ ($N$ is the Brunt-Väisälä frequency), which is close to a neutral profile, and winds that increase slightly with depth across it (from 0.5 to 10 bar). In addition, the wind structure in our simulation changed very little as the disturbance progressed, in agreement with what we observe at cloud level.

GWSs have been observed to occur once per Saturnian year in the northern hemisphere summertime season[5,9,10] (see Supplementary Information). The 2010 event occurred in the much earlier springtime season within the same westward jet as the 1903 event[5,9–11,14], pointing to seasonal insolation as their triggering mechanism. This is puzzling, as seasonal temperature changes occur only above ~500 mbar altitude (as shown by solar radiation penetration in Saturn's atmosphere[24] and by thermal infrared measurements[21,25]); this is much higher than the 10–12 bar level of the storm source[5,6]. The zonal wind profile at the 0.5–1 bar level does not change over one Saturnian year[1,7] (Fig. 3), ruling out a related seasonal dynamical instability. So the deep trigger could then be induced by seasonal changes in the upper troposphere temperature gradients directly affecting the deep vertical motions or indirectly modifying the pattern of meridional cell circulations between opposed jets proposed to exist at different altitudes in the weather layer[1,26].

The observed properties of the GWS and its modelling suggest that the storm is fuelled by a reservoir of water vapour at the 10–12 bar level in the westward jet, together with a sustained strong convergence[5,6]. The storm head extends downwards from ~260 km below the cloud tops, and across the weather layer (0.5–10 bar), where zonal winds stay constant (or increase slightly) with depth, in agreement with both previous observations and models of mid-latitude Saturnian vortices[27,28] and wind speed measurements at the 2–3 bar level[29]. The huge planetary-scale disturbance GWS triggered by the storm did not modify the westward zonal jet structure substantially; this indicates that Saturn's tropospheric winds are robust and extend well below the sunlight penetration level. Taken together, our data favour the hypothesis that these tropospheric winds have a deep origin[1], as is the case for Jupiter's winds[12].

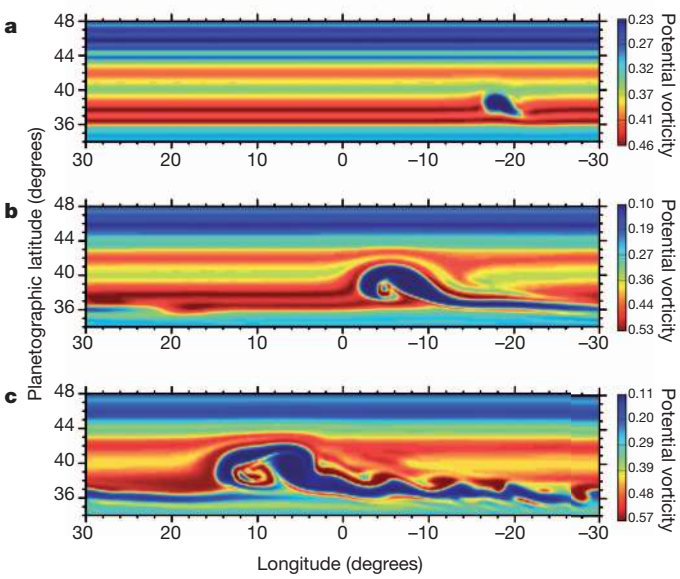


**Figure 4 | Models of the GWS planetary-scale disturbance.** Shown are nonlinear EPIC simulations[22] of the onset and initial evolution of the potential vorticity field associated with the storm at pressure level 850 mbar at days 1 (**a**), 6 (**b**) and 12 (**c**). To simulate the GWS, we introduced on Saturn's wind flow a vertically extended continuous heat source column with a power of 500 W m$^{-2}$ and a Gaussian shape of size 0.6°. The constant injection of heat from altitude levels 0.5 to 10 bar mimics the continuous latent heat released upward by the convective storm. The model atmosphere depends on the vertical and meridional structure of the zonal wind velocity $U(y,z)$, and on the vertical thermal structure represented here by the static stability or Brunt-Väisälä frequency $N(P)$, where we use $z$ or pressure $P$ as vertical coordinates and $y$ as meridional coordinate. The wind field structure is modelled as a product of two functions: $U(y,p) = u_h(y)u_v(P)$, where $u_h(y)$ is the wind profile at the cloud tops ($P_0$ = 500 mbar, refs 1, 12, Fig. 3), and $u_v(P) = 1 + m \ln(P/P_0)$ is a non-dimensional vertical amplitude factor. We tested different values for slope $m$ above and below $P_0$ = 500 mbar (refs 27, 28). Similarly, for the thermal structure we adopted $N(P)$ increasing with altitude for $P < 500$ mbar (ref. 26) and $N(P)$ = constant for $P > 500$ mbar. The horizontal domain for the simulations was a 60° × 15° channel with resolution 0.23° per pixel, and the vertical domain consisted of 8 layers from 10 mbar to 10 bar. The simulation that best resembles the evolution of the observed cloud field was obtained for a low static stability $N^2 = 0.03 \times 10^{-4}\,s^{-2}$ ($P > 500$ mbar) and for zonal winds that have slightly positive vertical shear ($m = 0.1$), that is, winds increasing below the cloud tops across the altitude range from $P$ = 0.5 to10 bar. Longitude is given in an arbitrary longitude system centred in the simulation domain.

**Received 26 February; accepted 10 May 2011.**


1. Del Genio, A. D. *et al.* in *Saturn from Cassini-Huygens* (eds Dougherty, M., Esposito, L. & Krimigis, T.) 113–159 (Springer, 2009).
2. Porco, C. C. *et al.* Cassini imaging science: initial results on Saturn's atmosphere. *Science* **307,** 1243–1247 (2005).
3. Dyudina, U. A. *et al.* Lightning storms on Saturn observed by Cassini ISS and RPWS during 2004–2006. *Icarus* **190,** 545–555 (2007).
4. Fischer, G. *et al.* Analysis of a giant lightning storm on Saturn. *Icarus* **190,** 528–544 (2007).
5. Sánchez-Lavega, A. & Battaner, E. The nature of Saturn's atmospheric Great White Spots. *Astron. Astrophys.* **185,** 315–326 (1987).
6. Hueso, R. & Sánchez-Lavega, A. A. Three-dimensional model of moist convection for the giant planets II: Saturn's water and ammonia moist convective storms. *Icarus* **172,** 255–271 (2004).
7. Sánchez-Lavega, A., Rojas, J. F. & Sada, P. V. Saturn's zonal winds at cloud level. *Icarus* **147,** 405–420 (2000).
8. Sayanagi, K. M. & Showman, A. P. Effects of a large convective storm on Saturn's equatorial jet. *Icarus* **187,** 520–539 (2007).
9. Sánchez-Lavega, A. *et al.* The Great White Spot and disturbances in Saturn's equatorial atmosphere during 1990. *Nature* **353,** 397–401 (1991).
10. Sánchez-Lavega, A., Lecacheux, J., Colas, F. & Laques, P. Temporal behavior of cloud morphologies and motions in Saturn's atmosphere. *J. Geophys. Res.* **98** (E10), 18857–18872 (1993).
11. Barnet, C. D., Westphal, J. A., Beebe, R. F. & Huber, L. F. Hubble Space Telescope observations of the 1990 equatorial disturbance on Saturn: zonal winds and central meridian albedos. *Icarus* **100,** 499–511 (1992).
12. Sánchez-Lavega, A. *et al.* Depth of a strong jovian jet from a planetary-scale disturbance driven by storms. *Nature* **451,** 437–440 (2008).
13. Fischer, G. *et al.* A giant thunderstorm on Saturn. *Nature* doi:10.1038/nature10205 (this issue).
14. Sánchez-Lavega, A. Motions in Saturn's atmosphere: observations before Voyager encounters. *Icarus* **49,** 1–16 (1982).
15. Beebe, R. F., Barnet, C., Sada, P. V. & Murrell, A. S. The onset and growth of the 1990 equatorial disturbance on Saturn. *Icarus* **95,** 163–172 (1992).
16. Seidelmann, P. K. *et al.* Report of the IAU/IAG working group on cartographic coordinates and rotational elements: 2006. *Celestial Mech. Dyn. Astron.* **98,** 155–180 (2007).
17. Sánchez Lavega, A. *et al.* Large-scale storms in Saturn's atmosphere during 1994. *Science* **271,** 631–634 (1996).
18. Acarreta, J. R. & Sánchez-Lavega, A. Vertical cloud structure in Saturn's 1990 equatorial storm. *Icarus* **137,** 24–33 (1999).
19. Pérez-Hoyos, S., Sánchez-Lavega, A., French, R. G. & Rojas, J. F. Saturn's cloud structure and temporal evolution from ten years of Hubble Space Telescope Images (1994–2003). *Icarus* **176,** 155–174 (2005).
20. West, R. A., Baines, K. H., Karkoschka, E. & Sánchez-Lavega, A. in *Saturn from Cassini-Huygens* (eds Dougherty, M., Esposito, L. & Krimigis, T.) 161–179 (Springer, 2009).
21. Fletcher, L. N. *et al.* Seasonal change on Saturn from Cassini CIRS observations, 2004–2009. *Icarus* **208,** 337–352 (2010).
22. Dowling, T. E. *et al.* The explicit planetary isentropic-coordinate (EPIC) atmospheric model. *Icarus* **132,** 221–238 (1998).
23. Read, P. L. *et al.* Mapping potential vorticity dynamics on Saturn: zonal mean circulation from Cassini and Voyager data. *Planet. Space Sci.* **57,** 1682–1698 (2009).

24. Pérez-Hoyos, S. & Sánchez-Lavega, A. Solar flux in Saturn's atmosphere: maximum penetration and heating rates in the aerosol and cloud layers. *Icarus* **180,** 368–378 (2006).
25. Li, L. *et al.* Saturn's emitted power. *J. Geophys. Res.* **115,** E11002, doi:10.1029/2010JE003631 (2010).
26. Barnet, C. D., Beebe, R. F. & Conrath, B. J. A seasonal radiative-dynamic model of Saturn's troposphere. *Icarus* **98,** 94–107 (1992).
27. García-Melendo, E., Sánchez-Lavega, A. & Hueso, R. Numerical models of Saturn's long-lived anticyclones. *Icarus* **191,** 665–677 (2007).
28. del Río-Gaztelurrutia, T., Legarreta, J., Hueso, R., Pérez-Hoyos, S. & Sánchez-Lavega, A. A long-lived cyclone in Saturn's atmosphere: observations and models. *Icarus* **209,** 665–681 (2010).
29. Choi, D. S., Showman, A. P. & Brown, R. H. Cloud features and zonal wind measurements of Saturn's atmosphere as observed by Cassini/VIMS. *J. Geophys. Res.* **114,** E04007, doi:10.1029/2008JE003254 (2009).
30. Hueso, R. *et al.* The International Outer Planets Watch atmospheres node database of giant planets images. *Planet. Space Sci.* **58,** 1152–1159 (2010).

**Supplementary Information** is linked to the online version of the paper at www.nature.com/nature.

**Acknowledgements** A.S.-L., T.d.R.-G., R.H., J.L., J.M.G.-F., E.G.-M. and J.F.S.-R. are supported by the Spanish MICIIN, by FEDER and by Gobierno Vasco. We thank S. Pérez-Hoyos for initial support of this study and M. Alises and A. Guijarro for taking the Calar Alto Observatory images (CAHA and MPG/CSIC). E.G.-M. used computing facilities at CESCA (Barcelona) supported by MICIIN. L.N.F. is supported by a Glasstone fellowship at the University of Oxford. The International Outer Planet Watch (IOPW) Team and other individual contributors listed in Supplementary Information provided most of the images used for tracking in this study; these images were complemented in some cases with images taken from contributors to the ALPO Japan (Association of Lunar and Planetary Observers) database (http://alpo-j.asahikawa-med.ac.jp/indexE.htm).

**Author Contributions** A.S.-L. coordinated the study and performed the motion and wind measurements and the interpretation. T.d.R.-G. performed the photometric measurements and filter calibrations. R.H. measured the storm growth rate and with J. Legarreta coordinated the IOPW database. J.M.G.-F. prepared the map projections and image search. J.F.S.-R. performed the radiative transfer calculations. E.G.-M. and J. Legarreta performed the EPIC simulations. F.C. and J. Lecacheux provided the Pic-du-Midi photometric images. L.N.F. provided data on the thermal structure of the storm. D.B.-N. provided the photometric images obtained at Calar Alto Observatory, and D.P. provided photometric images at selected wavelengths. All these authors discussed the results and commented on the manuscript. Contributors to the IOPW-PVOL database are listed at the end of this Letter.

**Author Information** Reprints and permissions information is available at www.nature.com/reprints. The authors declare no competing financial interests. Readers are welcome to comment on the online version of this article at www.nature.com/nature. Correspondence and requests for materials should be addressed to A.S.-L. (agustin.sanchez@ehu.es).

**The International Outer Planet Watch (IOPW) Team**

T. Akutsu[1], T. Barry[2], J. Beltran[3], S. Buda[4], B. Combs[5], F. Carvalho[6], P. Casquinha[7], M. Delcroix[8], S. Ghomizadeh[1], C. Go[9], J. Hotershall[10], T. Ikemura[1], G. Jolly[11], A. Kazemoto[1], T. Kumamori[1], M. Lecompte[12], P. Maxson[13], F. J. Melillo[14], D. P. Milika[15], E. Morales[16], D. Peach[17], J. Phillips[18], J. J. Poupeau[19], J. Sussenbach[20], G. Walker[21], S. Walker[22], T. Tranter[23], A. Wesley[24], T. Wilson[25] & K. Yunoki[1]

[1]ALPO-Japan (Kansai branch) 520-0242, 4-8-11, Honkatata Otsu-city, Shiga, Japan, and IOPW at Escuela Técnica Superior de Ingeniería de Bilbao, Ald. Urquijo s/n 48013 Bilbao, Spain. [2]406 Bromide Street, Broken Hill, New South Wales 2880, Australia. [3]Dr Jose Prades n.7, 12511 Rossell, Castellon, Spain. [4]31 Raglan Street, St Kilda East, 3183 Melbourne, Australia. [5]606 Frank Powell Road, Buena Vista, Georgia 31803, USA [6]Centro de Estudos do Universo, 17380-000 Brotas, Brazil. [7]Rua Gil Eanes Ite. 216, 2° dto, Portais da Arrábida, Quinta do Anjo, 2850-745 Palmela, Portugal. [8]2, rue de l'Ardache, 31170 Tournefeuille, France. [9]Physics Department, University of San Carlos, Nasipit, Talamban, 6000 Cebu City, Philippines. [10]21 Tarcutta Street Cleveland, Brisbane, Queensland 4163, Australia. [11]848 S. Rosemont Ct., Gilbert, Arizona 85296, USA. [12]51, Frogmore Close, Slough, SL1 9BN, UK. [13]17109 N. Eureka Trail, Surprise, Arizona 85374, USA. [14]14 Glen-Hollow Dr., E-16, Holtsville, New York 11742, USA. [15]12 Capri Crescent, Sellicks Beach, South Australia 5174, Australia. [16]HC2 PO Box 20031, Aguadilla, 00603 Puerto Rico. [17]28 North Road, Selsey, West Sussex, PO20 0BW, UK. [18]1280 Johnnie Dodds Blvd, Suite 104, Mt Pleasant, South Carolina 29464, USA. [19]6 Grande Rue, 91470 Pecqueuse, France. [20]Meekrap-oord 3, 3991 VE Houten, The Netherlands. [21]632 Byars Drive, Macon, Georgia 31210, USA. [22]294 Myrtle Street, Manchester, New Hampshire 03104, USA. [23]8 Ellalong Street, Kurri Kurri, New South Wales 2327, Australia. [24]PO Box 409, Campbell, Australian Capital Territory 2612, Australia. [25]5755 North Point Parkway, Suite 219m, Alpharetta, Georgia 30022, USA.